Journal of Applied Polymer Science

Thermal and Mechanical Properties of PES/PTFE Composites and Nanocomposites

Maria Cristina Righetti,[1] Alessia Boggioni,[1] Michele Laus,[2] Diego Antonioli,[2] Katia Sparnacci,[2] Luca Boarino[3]

[1]Istituto per i Processi Chimico-Fisici, Consiglio Nazionale delle Ricerche, Via G. Moruzzi 1, 56124 Pisa, Italy
[2]Dipartimento di Scienze e Innovazione Tecnologica (DISIT), Viale T. Michel 11, Università del Piemonte Orientale "A. Avogadro", INSTM, UdR Alessandria, 15121 Alessandria, Italy
[3]NanoFacility Piemonte, Electromagnetism Division, Istituto Nazionale di Ricerca Metrologica, Strada delle Cacce 91 - 10135 Torino, Italy
Correspondence to: M.C. Righetti (E - mail: cristina.righetti@ipcf.cnr.it)

ABSTRACT: Polyethersulphone/polytetrafluoroethylene (PES/PTFE) nanocomposites and composites were prepared by precipitation of PES into a PTFE latex-containing nanoparticles. Different samples were obtained by varying the relative ratio between PES and PTFE. The complex crystallization process, discussed within the fractionated crystallization frame, allowed to identify and quantify different dispersion degree of the PTFE nanoparticles within the PES matrix. The different samples were thus divided into nanocomposite and composites. The effect of crystalline PTFE domains on the mobility of PES was investigated and discussed. The dynamic-mechanical behavior was explained in terms of the particle aggregation state. The mechanical properties of the PES/PTFE composites were found to depend on both the dispersion and the concentration of the PTFE nanoparticles. In the glassy state the stiffness of the materials was found to increase with the dispersion degree, resulting higher for the nanocomposite with respect to composites. On the contrary, in the rubbery state the modulus was found proportional to the PTFE nanoparticles concentration, resulting higher in the composites with respect to the nanocomposite. © 2013 Wiley Periodicals, Inc. J. Appl. Polym. Sci. 130: 3624–3633, 2013

KEYWORDS: thermal properties; differential scanning calorimetry (DSC); mechanical properties

Received 23 April 2013; accepted 1 June 2013; Published online 26 June 2013
DOI: 10.1002/app.39613

INTRODUCTION

Over the past decade, extensive interest was addressed to thermally stable polymers due to the increasing demands for high performance polymers as replacement for metals or ceramics in automotive, aerospace and microelectronics industries. Aromatic polysulphones are one of the most successful classes of high performance polymers because of their thermal stability and excellent mechanical and electrical properties,[1] although processing difficulties and poor solubility in organic solvents, deriving from chain stiffness and strong intermolecular interactions, are often observed. Among these high performance materials, a good compromise between thermal stability and processability is provided by polyethersulphones (PES), as for example Radel A®. This resin, whose structure is in the Scheme 1, is widely employed for engineering applications, such as engine parts of racing cars and moulded parts for space shuttle. On the other hand, PTFE-based materials have a prominent position when applications where low friction coefficient, surface energy and dielectric constant, low refractive index, low flammability, low moisture adsorption and excellent thermal stability, and inertness are required.[2] The combination of these properties with those of PES would be highly desirable. However, the PTFE blending propensity with technopolymers is in general inadequate. The low surface energy prevents attachment and adhesion, thus resulting in low dispersion degrees and inefficient mechanical coupling among the various blend components. To enhance wettability and compatibility, PTFE surface modification approaches were developed with high reactive chemicals or high energy treatments like plasma or UV.[3,4] A mild alternative to produce compounds featuring a perfect distribution of PTFE particles is based on the preparation of core-shell particles in which the core is constituted by PTFE and the shell by the technopolymer of interest. A perfect dispersion of the PTFE nanoparticles can be anticipated when the matrix is constituted by the same polymer with which the shell is made up.[5,6] PTFE/PS,[7,8] PTFE/PMMA[9] and PTFE/polyacrylates[10–12] core-shell nanoparticles and nanocomposites were recently prepared using this approach. Unfortunately, this method cannot be employed when PTFE should be dispersed in preformed polymers. At the

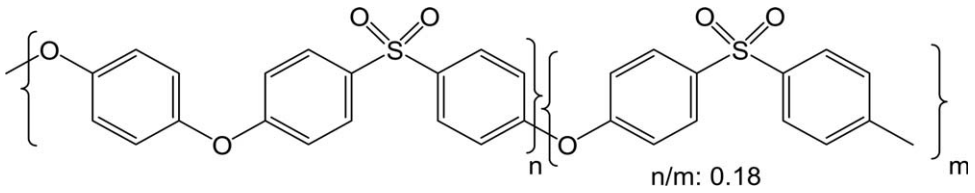

Scheme 1. Structure of polyethersulphone (PES).

same time, other conventional mixing techniques, like solution casting and coprecipitation blending cannot be used due to the low solubility of PTFE. In this respect, the precipitation of the preformed polymer in latex containing PTFE particles can be considered as an alternative to melt mixing. This approach was recently employed in the preparation of PTFE-containing composites and nanocomposites based on PES, where the mixing step was accomplished through PES precipitation into an aqueous dispersion containing PTFE nanoparticles.[13] Using this approach, PES/PTFE composites and nanocomposites were prepared featuring a perfect PTFE dispersion degree in certain compositional range.

Many investigations reveal that the glass transition temperature, the dynamics of the polymer chains, and the mechanical properties can be largely influenced by the incorporation of particles in the polymer matrix.[14–20] The addition of rigid particles may either ease or constrain the motion of the polymer chains, depending on the nature of the polymer-filler interactions. Attractive interactions at the polymer-filler interface generate a reduction in chain mobility, which may result in an enhancement of T_g.[14,15] Conversely, the absence of specific interactions may be responsible for a reduction of T_g, due to the improved segmental motions at the polymer-filler interface because of the extra free-volume contribution.[17,18] The dynamic-mechanical spectroscopy is frequently used in composites and nanocomposites characterization since it allows the measurement of stiffness and energy losses as a function of temperature. Dynamic-mechanical data generally show significant improvements in the storage modulus over a wide temperature range for a large number of polymer composite and nanocomposites.[19,20] All the thermal and mechanical properties are strongly affected by the degree and scale of filler dispersion, presenting a peculiar change when dispersion at nanoscale is achieved.

The aim of this contribution is to report on the effect of the addition of rigid PTFE particles on the properties of an amorphous thermoplastic PES, identified by the trade name Radel A®. The effect of the dispersion degree on the thermal and mechanical properties of the PES matrix is analyzed and discussed.

EXPERIMENTAL

Materials

PTFE latex consists of a bimodal mixture of spherical and rod-like particles. This latex was prepared as described in literature.[21]. PES (Radel A®) was provided by Solvay Solexis. 1-Methyl-2-Pyrrolidone (NMP) was purchased from Aldrich.

Nanoparticles Preparation

The PES/PTFE composites were prepared according to the procedure described in Ref. 13. First PES was dissolved at 50°C in NMP with concentration 4% w/w. Then the appropriate amount of PTFE latex (concentration 0.1951 g mL^{-1}) was introduced into a four necked 1 L reactor, equipped with mechanical stirrer, thermometer, condenser and inlet for the PES solution. Deionized water was added to reach the final volume of 460 mL. The diluted latex was then heated at 50°C under stirring at 300 rpm. After additional 15 min equilibrium time, 360 g of the NMP solution containing the PES were added dropwise to the PTFE latex with a total addition time of 3 hours. Then, the mixture was cooled and the organic solvent eliminated by repeated dialyses. All the PTFE/PES latexes were obtained following the above general procedure by varying the initial PTFE latex amount. Table I collects the details of the various preparations. A pure PES sample was also prepared by adding dropwise the PES solution into 400 mL of water at 50°C. Powder samples were recovered by drying overnight the water suspensions in a vacuum oven at 80°C.

Nanoparticles Characterization

Thermogravimetric analysis (TGA) was performed using a Mettler-Toledo thermobalance TGA/SDTA 851 at a scanning rate of 10°C min^{-1} from room temperature up to 800°C under nitrogen flow.

DSC measurements were performed with a Perkin-Elmer Differential Scanning Calorimeter DSC7. The instrument was

Table I. Synthesis Details

Sample	Volume of H_2O (mL)	Mass of solution of PES in NMP 4% w/w (g)	Volume of PTFE latex (mL)	PES estimated (wt %)	PTFE estimated (wt %)
PES	460.0	360.0	-	100	0
PES/PTFE 95/5	456.0	360.0	3.8	95	5
PES/PTFE 80/20	442.0	360.0	17.9	80	20
PES/PTFE 60/40	412.0	360.0	47.8	60	40

calibrated in temperature and energy with high purity standards (indium, naphthalene and cyclohexane) according to the procedure for standard DSC.[22] Dry nitrogen was used as purge gas at a rate of 30 mL min^{-1}. The investigation of the thermal behavior of all the samples was performed by cooling the samples at $-20°C\ min^{-1}$ from 350°C down to 180°C and successively reheating them up to 350°C at $+20°C\ min^{-1}$. From these measurements the T_gs of the samples were determined as the midpoint of the specific heat capacity step. A more detailed analysis of the crystallization and melting behavior of the PES/PTFE 80/20 sample was carried out by cooling and successively heating the sample at different rates: $-5°C\ min^{-1}$/$+5°C\ min^{-1}$, $-10°C\ min^{-1}$/$+10°C\ min^{-1}$ and $-20°C\ min^{-1}$/$+20°C\ min^{-1}$, respectively. To obtain precise heat capacity data, each measurement was accompanied by an empty pan run and a calibration run with sapphire under identical conditions.[22]

Dynamic-mechanical analyses were carried out using a dynamic mechanical analyzer Rheometric DMTA V, employing the single cantilever flexural geometry. A scanning rate of $4°C\ min^{-1}$ was chosen. The strain was sufficiently small to be within the linear viscoelastic range at the frequency of 1 Hz. The samples for the dynamic-mechanical analysis were prepared by introducing the powder polymer sample into a rectangular mould. The entire assembly was then placed between press plates with a nominal pressure of $4.9{\sim}10^7$ Pa and allowed to stand at room temperature for 20 min. The temperature was then raised to 350°C and the pressure slowly released to $4.9{\cdot}10^6$ Pa. After 15 min, the sample was quenched into cold water and recovered as rectangular 20 × 5 × 2 mm sheets.

Morphological investigation was performed using an Inspect F SEM-FEG (Field Emission Gun) microscope from FEI company, with a beam diameter of 3 nm, both on sample powders and on fractured specimens obtained from compact samples prepared as above described.

These samples were immersed in liquid nitrogen for 30 min and then immediately fractured. To avoid electron charging effects during SEM analysis, the samples were coated with 3 nm of gold, by means of a Cressington 108 Auto sputter coater in argon plasma atmosphere (0.15 mbar) with an emission current of 25 mA.

RESULTS AND DISCUSSION

Nanoparticles and Nanoparticles Mixture Composition and Morphology

The composition of the PTFE/PES nanoparticle mixtures, estimated by the feed composition, as reported in Table I, was confirmed by TGA. Figure 1 reports the TGA curves of the nanoparticle mixtures and, for comparison, the TGA curve of PTFE and the one of the pure PES prepared by precipitating the PES solution of into water. The main weight losses of PTFE and PES are both centred at 550°C. At 800°C, the residue of PES is 38%. No residue was observed for PTFE. From the different residue values, the average samples composition was estimated and resulted in good agreement with the one calculated on the base of the recipes.

The morphology of the powder samples was studied by SEM. Figure 2 reports, as typical examples, the SEM micrographs of

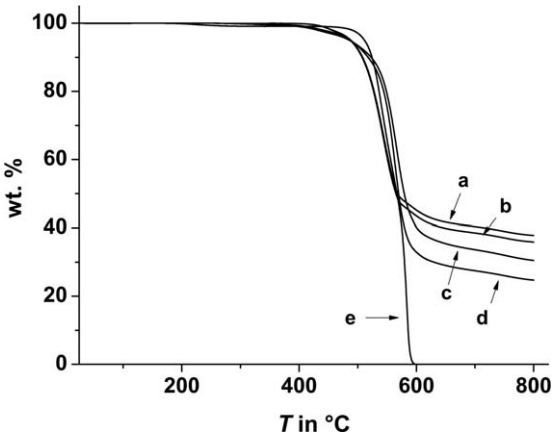

Figure 1. TGA curves of PES (a), PES/PTFE 95/5 (b), PES/PTFE 80/20 (c), PES/PTFE 60/40 (d) and PTFE, and (e) at $10°C\ min^{-1}$ under nitrogen flow.

pure PTFE and PES as well as PES/PTFE 80/20 and PES/PTFE 60/40. PTFE sample is a bimodal mixture consisting of spherical (21 wt %) and of rod-like (79 wt %) particles [Figure 2(a)]. The diameter of the spherical particles is 41 ± 9 nm. The rod-like particles are characterized by a length (L) of 141 ± 60 nm and a diameter (D) of 41 ± 8 nm, thus giving an average aspect ratio (L/D) of 3.6 ± 1.5 nm. The PES sample is constituted by spherical-like particles with an average diameter of 150 ± 60 nm [Figure 2(b)]. The SEM images of PES/PTFE 80/20 and PES/PTFE 60/40, illustrated in Figure 2(c,d), appear a combination of those of the two pure components, although the rod-like particles of PTFE are difficult to be clearly distinguished. This is due to the fact that only the particles that lie horizontally can be identified whereas those oriented vertically are not distinguishable since their minor axis is approximately equal to the radius of many spherical particles.

Scanning electron microscopy was used also to investigate the microstructure of PTFE/PES samples prepared by compression moulding and cryofractured. Figure 3 shows the fractured surface micrographs of PES and its composites with PTFE. In case of PES, brittle fracture with smooth surfaces occurs. In contrast, in case of samples PES/PTFE 80/20 and PES/PTFE 60/40, ductile fracture with significant localized deformation in the form of fibrils is observed. For the former sample, the fibrils are 30–40 nm in diameter and can measure few microns in length whereas, for the latter sample, the fibrils are 50–150 nm in diameter and measure several tens of microns. In addition, the surface density of fibrils in case of PES/PTFE 60/40 is substantially higher than for PES/PTFE 80/20. The formation of fibrils in PTFE has received significant interest in the literature because fibrils were shown to provide a mechanism to dissipate energy and stabilize a crack tip by bridging.[23–25] The stability of PTFE fibrils was found primarily determined by temperature and crystalline phase with additional dependence on loading rate and microstructure anisotropy. The present data further stress the pronounced tendency of PTFE particles toward fibrillation and indicates that individual fibers can be obtained from the cold coalescence of adjacent particles. In addition, the homogeneous distribution of PTFE fibrils at the cryofractured surfaces

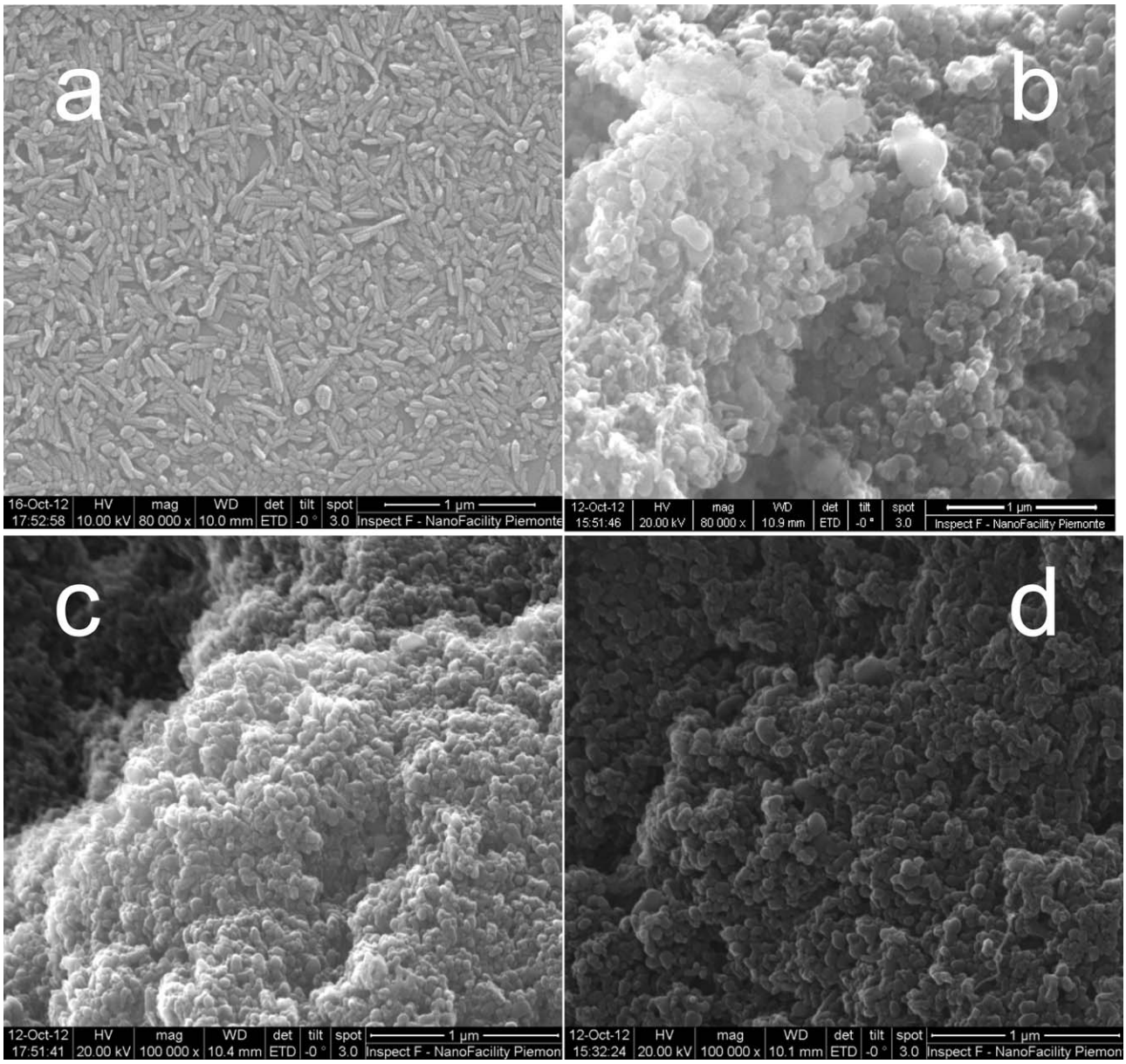

Figure 2. SEM micrographs of PTFE (a), PES (b), PES/PTFE 80/20 (c), and PES/PTFE 60/40 (d).

confirms the homogeneous distribution of PTFE nanoparticles within the composites.

Glass transition, Crystallization, and Melting Behavior

The specific heat capacities (c_p) curves of PES, PES/PTFE 95/5, PES/PTFE 80/20, PES/PTFE 60/40 and PTFE, measured at 20°C min^{-1} after cooling at −20°C min^{-1}, are shown in Figure 4, whereas the corresponding cooling c_p curves are depicted in Figure 5. It is worth noting that the specific heat capacity is positive for both crystallization and melting, since in the first case enthalpy decreases as temperature decreases, whereas in the second case enthalpy increases as the temperature raises.

The specific heat capacity curves of PES, PES/PTFE 95/5, PES/PTFE 80/20, and PES/PTFE 60/40 upon cooling and heating reveal a step in the range 220–240°C, which corresponds approximately to the bulk glass transition (T_g) of PES.[1] The glass transition of PTFE, located at much lower temperatures, approximately −70°C,[26] generally cannot be observed calorimetrically.[27] Above the melting of PTFE, the experimental specific heat capacity agrees with the thermodynamic c_p of liquid PTFE, as taken from ATHAS databank.[26] (The thermodynamic c_p data of PTFE are depicted in Figures 4 and 5 as dotted lines.) Conversely, the experimental c_p of the solid and liquid PES results slightly higher than the tabulated thermodynamic c_p, probably because the Radel A® used in the present study contains also monomeric units with oxy-phenylene groups.[28] Figures 4 and 5 show that in the glassy state the specific heat capacity of PES is higher than the specific heat capacity of PTFE. Accordingly, the specific heat of PES/PTFE samples shifts progressively toward lower values with increasing the PTFE content.

Applied Polymer SCIENCE

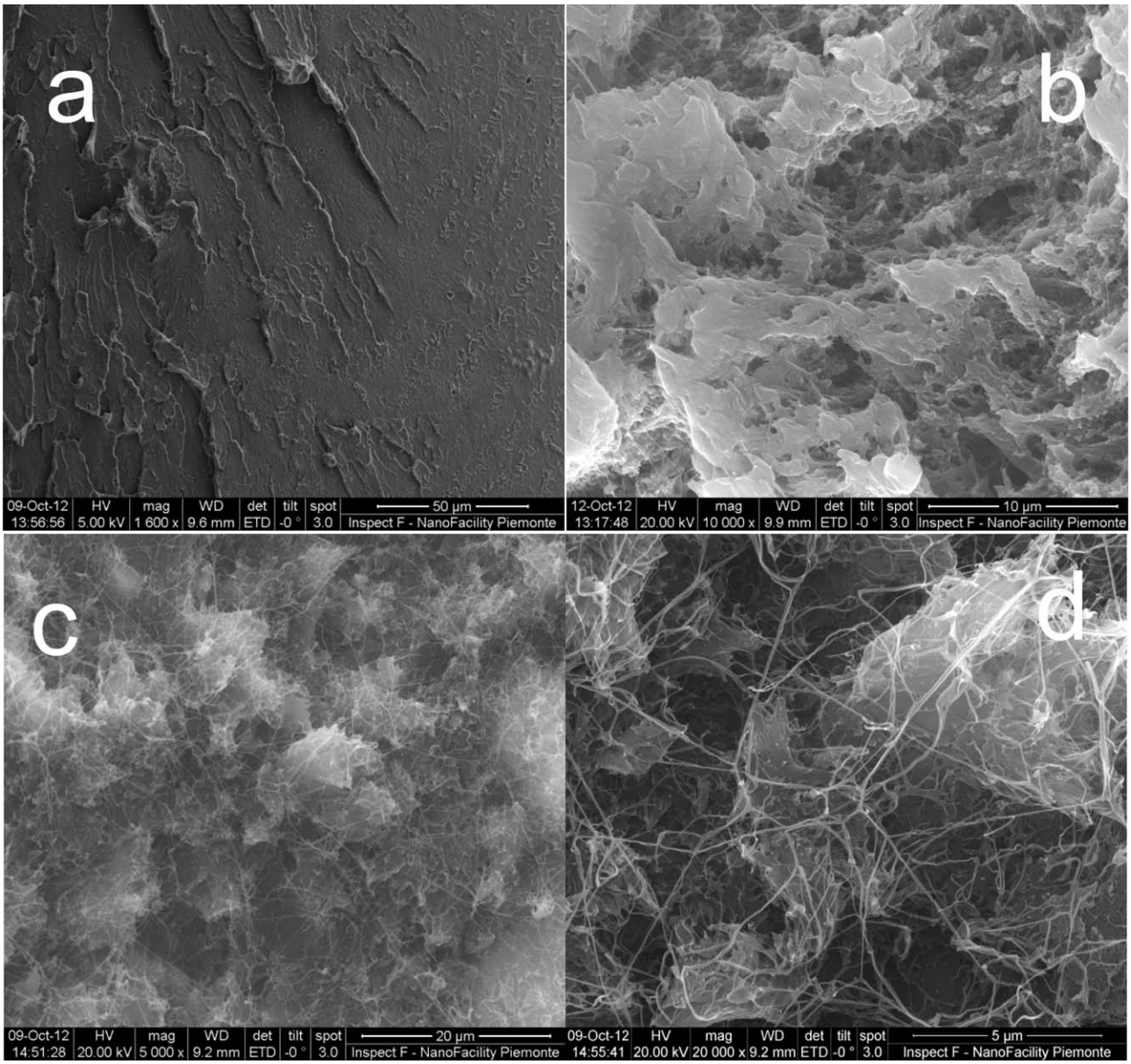

Figure 3. SEM micrographs of cryofractured surfaces of PES (a), PES/PTFE 80/20 (b), and PES/PTFE 60/40 (c and d).

At temperatures higher than the PES glass transition, a number of transitions can be evidenced in the c_p curves of PES/PTFE 95/5, PES/PTFE 80/20, PES/PTFE 60/40, and PTFE. During cooling, one or two major exotherms can be observed, whereas a single melting peak appears during the heating scan. As PES is a totally amorphous polymer,[1] the exothermic and endothermic events must be associated to PTFE. The occurrence of complex PTFE crystallization processes was described for several systems, including also PTFE/polyamide 6, PTFE/polyacrylates, PTFE/polystyrene and PTFE/polymethylmethacrylate core-shell systems.[7–13,29]

This behavior was rationalized within the frame of the fractionated crystallization mechanism. It is a characteristic of crystalline polymers to exhibit multiple crystallization transitions when dispersed as small particles,[30] as it may occur in some polymer blends[31,32] or microphase separated block copolymers.[33] If the number of the dispersed particles is much greater than the number of heterogeneities that usually nucleate the polymer in bulk, the polymer crystallization results activated at different degrees of undercooling and occurs in one or more stages because of different nucleation mechanisms.[34] The exotherm that is observed at 310°C for the samples PES/PTFE 80/20 and PES/PTFE 60/40 is the result of the crystallization of very large clusters of PTFE particles that, after the preliminary fusion, organize into micrometer-sized domains. In fact the crystallization of plain PTFE occurs at the same temperature range. This crystallization event, which starts with a heterogeneous nucleation mechanism, seems to occur down to approximately 280°C, which results in the growth of progressively less

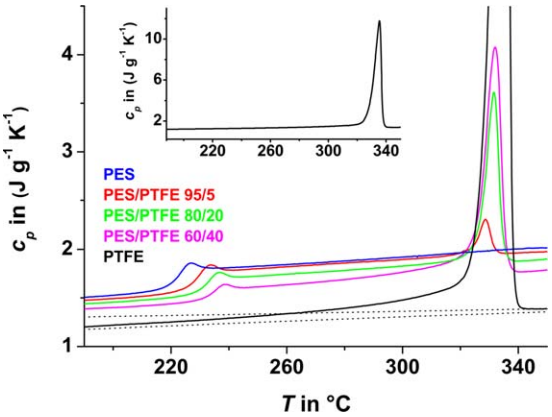

Figure 4. Specific heat capacity (c_p) of PES, PES/PTFE 95/5, PES/PTFE 80/20, PES/PTFE 60/40 and PTFE upon heating at +20°C min^{-1} after cooling at −20°C min^{-1}. The dotted lines are the thermodynamic solid and liquid c_p of PTFE, as taken from ATHAS databank.[26] In the inset the entire c_p curve of PTFE is reported. [Color figure can be viewed in the online issue, which is available at wileyonlinelibrary.com.]

perfect crystals. Conversely, the exotherm at about 275°C, which is observed for the PES/PTFE 95/5 and PES/PTFE 80/20 samples, can originate from crystal growth occurring according to a homogeneous nucleation mechanism, when it involves PTFE nanoparticles dispersed individually in the PES matrix. Thus the PES/PTFE 60/40 sample crystallizes exclusively according to a heterogeneous nucleation mechanism, the PES/PTFE 80/20 sample exhibits crystallization from both heterogeneous and homogeneous nucleation mechanisms, whereas the crystal growth for PES/PTFE 95/5 sample occurs almost completely according to a homogeneous nucleation mechanism. (Actually also the PES/PTFE 95/5 sample exhibits a broad and small crystallization event in the range 320°C $< T <$ 280°C, but it is of very small intensity and therefore negligible with respect to the one that is observed at 275°C.)

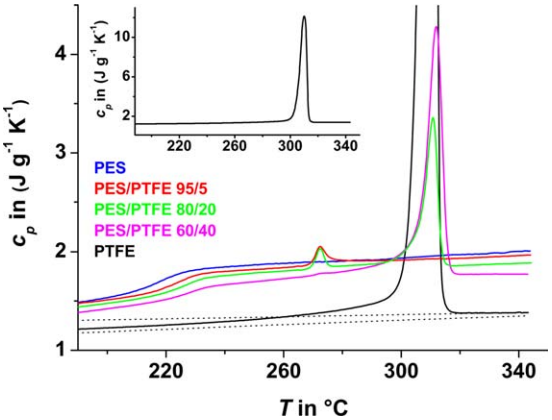

Figure 5. Specific heat capacity (c_p) of PES, PES/PTFE 95/5, PES/PTFE 80/20, PES/PTFE 60/40 and PTFE upon cooling at −20°C min^{-1}. The dotted lines are the thermodynamic solid and liquid c_p of PTFE, as taken from ATHAS databank.[26] In the inset the entire c_p curve of PTFE is reported. [Color figure can be viewed in the online issue, which is available at wileyonlinelibrary.com.]

Table II. Phase Composition in Weight Fractions and Glass Transition Temperature Data

Sample	$w_{C,nano}$	$w_{C,micro}$	$w_{A,PTFE}$	$w_{A,PES}$	T_g (°C)
PES	-	-	-	1.0	222
PES/PTFE 95/5	0.02	-	0.03	0.95	229
PES/PTFE 80/20	0.01	0.13	0.06	0.80	230
PES/PTFE 60/40	-	0.25	0.15	0.60	231

The crystal fraction that develops at about 275°C, as it derives from PTFE nanoparticles dispersed individually in the PES matrix, is a crystalline nanophase, whereas the crystal fraction that grows at about 310°C can be defined as a crystalline microphase, as it originates from large clusters of PTFE particles that, after the preliminary fusion, organize into micrometer-sized domains. The weight fractions of the PTFE crystalline nanophase ($w_{C,nano}$) and microphase ($w_{C,micro}$) in the PES/PTFE samples, calculated from the ratios between the experimental crystallization heats from heterogeneous and homogeneous nucleation and the enthalpy of crystallization of 100% crystalline PTFE (78.9 J g^{-1} at 275°C and 80.9 J g^{-1} at 310°C, respectively),[26] are collected in Table II, together with the weight fractions of the amorphous PTFE and PES phases ($w_{A,PTFE}$ and $w_{A,PES}$, respectively). From the values reported in Table II it is evident that when the PTFE amount is low (5 wt %), a perfect PTFE nanoparticle dispersion is obtained, which results in a weight fraction of the crystalline nanophase slightly <50% of the total PTFE. Partial aggregation is observed when PTFE concentration is 20 wt %, as proven by the value of the weight fraction of the crystalline nanophase, which results lower with respect to the PES/PTFE 95/5. Conversely, extensive aggregation is found for the sample PES/PTFE 60/40. In this case, crystalline nanophase is completely absent. As only PTFE crystalline nanophase is present in the sample PES/PTFE 95/5, it can be defined a nanocomposite, unlike the sample PES/PTFE 60/40, which can be considered as a composite, as the PTFE crystalline fraction is a microphase. The sample PES/PTFE 80/20 contains both PTFE crystalline nanophase and microphase, but because of the much higher microphase weight fraction, can be regarded mainly as a composite.

The peak temperature of the fusion of the PTFE crystals is located around 330°C: at 335°C for plain PTFE and at 332°C for both PES/PTFE 60/40 and PES/PTFE 80/20. The peak temperature for PES/PTFE 95/5 occurs a few degrees below, at 329°C (Figure 4). Since crystals from both homogeneous and heterogeneous nucleation are present in the PES/PTFE 80/20, the melting process of this sample was further investigated through experiments with different cooling and heating rates. Figure 6(A) shows the c_p curves recorded during cooling at −5°C min^{-1}, −10°C min^{-1}, and −20°C min^{-1} and Figure 6(B) the corresponding c_p curves obtained during the successive heating at +5°C min^{-1}, +10°C min^{-1}, and +20°C min^{-1}, respectively. As expected, with increasing the cooling rate, the undercooling for the crystallization process increases and both the exotherms shift to lower temperatures. Also the sum of the

Applied Polymer SCIENCE

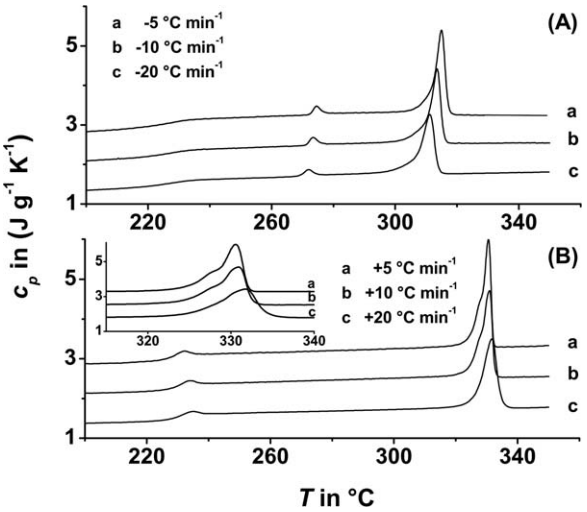

Figure 6. (A) Specific heat capacity c_p of PES/PTFE 80/20 upon cooling at $-5°C\ min^{-1}$, $-10°C\ min^{-1}$, and $-20°C\ min^{-1}$, respectively and (B) upon heating at $+5°C\ min^{-1}$, $+10°C\ min^{-1}$, and $+20°C\ min^{-1}$. The ordinate values refer only to curve c. Curves a and b are shifted vertically for the sake of clearness. In the insert an enlargement of the c_p curves in the melting region is reported.

crystallization exotherm areas, normalized to the PTFE content, reduces with increasing the cooling rates, passing from 60.7 J g_{PTFE}^{-1} at $-5°C\ min^{-1}$ to 54.1 J g_{PTFE}^{-1} at $-20°C\ min^{-1}$. A splitting of the melting process becomes evident as the heating rate is reduced [see enlargement in Figure 6(B)], thus suggesting that the two different nucleation mechanisms give rise to different populations of PTFE crystals with melting peaks spaced by approximately 3°C. As the depression of the melting point in confined materials is a well-known phenomenon,[35] the shoulder at lower temperature should correspond to the fusion of confined nanocrystals, whereas the more intense peak could be related to the melting of continuous or inter-connected PTFE crystalline domains.

The glass transition of the PES/PTFE samples increases with increasing the PTFE content, as shown in Figure 4 and reported in Table II. The specific heat increment at T_g (Δc_p) of PES is 0.20 J $g^{-1}\ K^{-1}$, whereas for PES/PTFE 95/5, PES/PTFE 80/20, and PES/PTFE 60/40 is 0.19 J $g^{-1}\ K^{-1}$, 0.16 J $g^{-1}\ K^{-1}$, and 0.12 J $g^{-1}\ K^{-1}$, respectively. When the Δc_ps of the mixtures are normalized to the PES concentration, the specific heat increment of plain PES is obtained, which could suggest that the observed glass transition originates from the chain motions of the only PES component.

As observed in some inorganic filled composites,[36–39] dispersed rigid regions can disturb the molecular rearrangements involved during the glass transition owing to strong molecular interactions. The presence of a less mobile polymer interfacial layer at the domain boundaries can lead to restrictions of the cooperative motions of the vitrifying polymer, thus resulting in a higher T_g. A parallel reduction of the specific heat increment Δc_p, which can be sometimes detected, was ascribed to the existence of an immobilized fraction that does not devitrifies at T_g.[39] As above reported, a Δc_p reduction was not observed for the system PES/PTFE with increasing the PTFE content, which proves the absence of strong interactions and of a rigid amorphous PES fraction at the PTFE domains boundaries. The presence of specific interactions between PES and PTFE can be excluded also from specific heat capacity considerations. When specific intermolecular interactions are not active, the specific heat capacity of the mixture (c_p), in the absence of latent heat, can be expressed as:[40]

$$c_p = w_{p1}c_{p1} + w_{p2}c_{p2} \quad (1)$$

where w_{pi} and c_{pi} are, respectively, the weight fraction and the specific heat capacity of the polymer *i*. The c_p values of PES/PTFE 95/5, PES/PTFE 80/20, and PES/PTFE 60/40, calculated according to eq. (1) in the glassy state, match perfectly the respective measured specific heat capacities. This means that the interactions that are established at the interface PES/PTFE are not strong directional specific interactions, but weaker interactions, probably dipole-induced dipole, as expected because of the zero PTFE dipole moment. Consequently, the increase of the glass transition temperature with the PTFE content has to be explained according to a totally different mechanism.

The presence of rigid domains can produce an elevation of the glass transition temperature also through a friction or "wall" effect. This hypothesis was used to explain the high temperature shift in the glass transition of poly(ethylene terephthalate) in a blend with polycarbonate.[41] Also for immiscible polystyrene/polypropylene blend, the increase in the polystyrene T_g with increasing the percentage of polypropylene, which crystallizes at higher temperature, was interpreted invoking a friction effect.[42] These effects could be responsible for the observed increase in the glass transition of PES in the present PES/PTFE system, in which the vitrification of PES takes place in the presence of rigid PTFE crystal domains. The rigid PTFE crystalline domains can obstruct the PES rearrangement motions through a frictional effect and exert constraints on the PES relaxation process. As a matter of fact, a perfect nanoparticle dispersion, obtained with the addition of a small PTFE weight percentage and characterized by a wide interfacial PES/PTFE area, produces a sharp increase of T_g, which passes from 222°C of plain PES to 229°C of PES/PTFE 95/5. A further addition of PTFE leads to a reduction of the interfacial area growth, as a consequence of partial nanoparticles aggregations. Therefore the T_g increase is proportionally smaller: a PTFE addition of 20 wt % and 40 wt % produces a T_g elevation respectively of 8°C and 9°C with respect to plain PES.

Dynamic-Mechanical Behavior

The dynamic-mechanical behavior of PES/PTFE samples was also studied. The analysis was performed in the linear viscoelasticity region between 50°C and the temperature at which the samples lost their dimensional stability. The curves of the storage modulus E' (the elastic component of viscoelastic response) as a function of temperature for PES and PES/PTFE samples are depicted in Figure 7(A), whereas Figure 7(B) shows the tan δ curves (E''/E' = ratio of energy dissipated to energy stored) as a function of temperature in the glass transition region. The dynamic storage modulus E' decreases with increasing temperature with a drop at about 230°C, corresponding to the glass

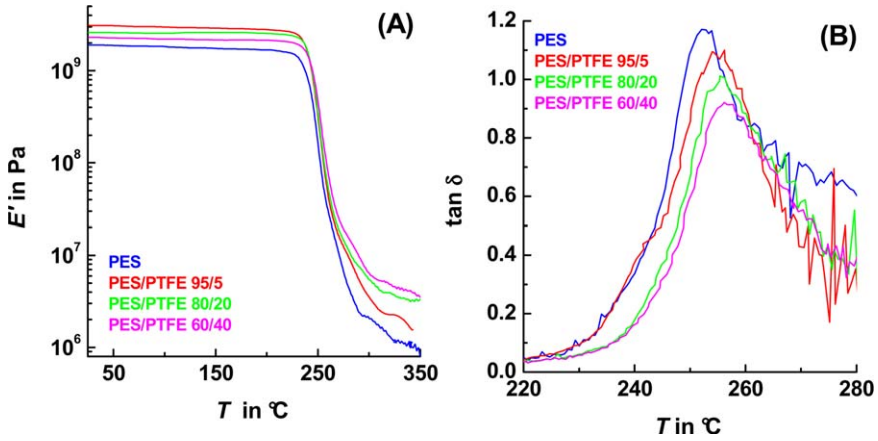

Figure 7. Trend of dynamic storage modulus E' (A) and trend of loss tangent tan δ (B) as a function of temperature for PES, PES/PTFE 95/5, PES/PTFE 80/20, and PES/PTFE 60/40 samples. [Color figure can be viewed in the online issue, which is available at wileyonlinelibrary.com.]

transition of the PES component. Figure 7(B) reveals that the glass transition temperature increases with increasing the PTFE concentration, in agreement with the DSC analysis, whereas the intensity of tan δ peak decreases with increasing PTFE content, as also reported for composites with glass and carbon fiber as reinforcement.[43,44]

The magnitude of the storage modulus in the glassy and rubbery regions depends differently on the PTFE weight fraction. In the glassy state the storage modulus increases from 1.9 GPa for plain PES to 3.1 GPa for PES/PTFE 95/5, then decreases to 2.6 GPa and 2.3 GPa as the PTFE amount increases to 20 wt % and 40 wt %, respectively. On the contrary in the rubbery region a monotonic modulus elevation from 1.2 MPa to 4.6 MPa is observed at 325°C with increasing the PTFE concentration. The different modulus trends are better illustrated in Figure 8(A,B), which show the storage modulus E' and the ratio E_c/E_m (where E_c and E_m are the storage moduli of the composites and PES matrix, respectively) as a function of PTFE weight fraction at 50°C, that is well below the PES glass transition, and at 325°C, that is in the rubbery region. In the glassy state the trend of the ratio E_c/E_m seems to be connected to the dispersion degree of the PTFE nanoparticles. The perfect dispersion of the nanoparticles that occurs in the nanocomposite PES/PTFE 95/5, at temperatures lower than T_g produces an increase in the storage modulus and in the stiffness with respect to plain PES. But with increasing the PTFE nanoparticles concentration, both the storage modulus and the ratio E_c/E_m decrease. This effect can be explained by assuming the presence of particles assembled into aggregates in the composites PES/PTFE 80/20 e PES/PTFE 60/40. At temperatures lower than T_g the matrix is able to exert forces great enough to produce motions on the contact points among the particles, thus decreasing the modulus and the ratio E_c/E_m. Conversely, at temperature higher than T_g, the matrix is too soft to exert forces sufficient to overcome the friction at the contact points.[45–47] Consequently, the aggregated particle are less mobile and the modulus and the ratio E_c/E_m increase with increasing the PTFE nanoparticles concentration, according to the classical theory of mechanical reinforcement exerted by rigid particles embedded in a polymeric matrix.[48]

CONCLUSIONS

The effect of crystalline PTFE domains on the mobility of PES was investigated and discussed. The absence of specific interactions at the interface PES/PTFE was demonstrated from specific

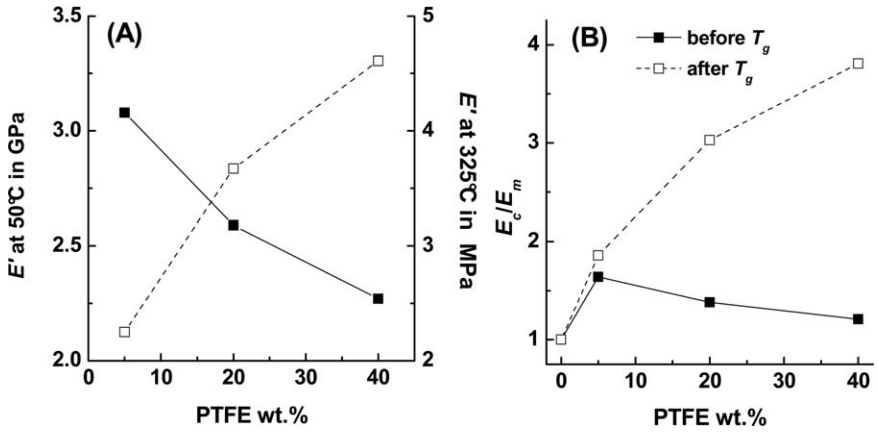

Figure 8. Trend of the storage modulus E' (A) and trend of the moduli ratio (E_c/E_m) (B) as a function of the PTFE wt % at 50°C (fully symbols) and at 325°C (open symbols). The lines are a guide to the eyes.

heat capacity considerations and the increase in the PES glass transition temperature observed with increasing the PTFE content was explained assuming a frictional effect exerted by the PTFE domains on the PES segmental motions. The rigid crystalline PTFE regions would hinder the cooperative rearrangements of the PES chains by acting like a wall.

The PTFE crystallization process was found quite complex and, depending on the sample composition, single or multiple crystallization exotherms were observed. This behavior, discussed within the fractionated crystallization frame, was revealing of the PTFE dispersion degree within the PES matrix. When the PTFE amount is low (5 wt %), a perfect nanoparticle dispersion is obtained and the PTFE crystalline phase is a nanophase. Partial aggregation is observed when PTFE concentration is 20 wt %, whereas extensive aggregation occurs for the sample PES/PTFE 60/40. On the base of dispersion degree of the PTFE nanoparticles within the PES matrix, the different samples were divided into nanocomposite and composites.

The dynamic-mechanical behavior was explained in terms of the particle aggregation state. The DMTA measurements revealed that the mechanical properties of the composites PES/PTFE depend on both the dispersion and the concentration of the PTFE nanoparticles. The magnitude of the storage modulus in the glassy and rubbery regions was found to depend differently on the PTFE weight fraction. In the glassy state the stiffness of the materials increases with the dispersion degree, resulting higher for the nanocomposite with respect to the composites. On the contrary, in the rubbery state the modulus was found proportional to the PTFE nanoparticles concentration, resulting higher in the composites with respect to the nanocomposite.

ACKNOWLEDGMENTS

Part of this work has been performed at NanoFacility Piemonte, INRiM, a laboratory supported by Compagnia di San Paolo.

REFERENCES

1. Mehmet-Alkan, A. A.; Biddlestone, F.; Hay, J. N. *Thermochim. Acta* **1995**, *256*, 123.
2. Tsibouklis, J; Nevell, G. T. *Adv. Mater.* **2003**, *15*, 647.
3. Ji, L. Y.; Kang, E. T.; Neoh, K. G.; Tan, K. L. *Langmuir* **2002**, *18*, 9035.
4. Konig, U.; Nitschke, M.; Menning, A.; Eberth, G.; Pilz, M.; Arnhold, C.; Simon, F.; Adam, G.; Werner, C. *Colloids Surf., B* **2002**, *24*, 63.
5. Okaniwa, M. *J. Appl. Polym. Sci.* **1998**, *68*, 185.
6. Suresh, K. I.; Pakula, T.; Bartsch, E. *Macromol. React. Eng.* **2007**, *1*, 253.
7. Giani, E.; Sparnacci, K.; Laus, M.; Palamone, G.; Kapeliouchko, V.; Arcella, V. *Macromolecules* **2003**, *36*, 4360.
8. Sparnacci, K.; Antonioli, D.; Deregibus, S.; Panzarasa, G.; Laus, M.; DeLeo, N.; Boarino, L.; Kapeliouchko, V.; Poggio, T. *Polym. Adv. Techol.* **2011**, *23*, 558.
9. Sparnacci, K.; Antonioli, D.; Deregibus, S.; Laus, M.; Poggio, T.; Kapeliouchko, V.; Palamone, G.; Zuccheri, G.; Passeri, R. *Macromolecules* **2009**, *42*, 3518.
10. Kapeliouchko, V.; Palamone, G.; Poggio, T.; Zuccheri, G.; Passeri, R.; Sparnacci, K.; Antonioli, D.; Deregibus, S.; Laus, M. *J. Polym. Sci. Part A, Polym. Chem.* **2009**, *47*, 2928.
11. Antonioli, D.; Deregibus, S.; Panzarasa, G.; Sparnacci, K.; Laus, M.; Berti, L.; Frezza, F.; Gambini, M.; Boarino .; Enrico, E.; Comoretto, D. *Polym. Int.* **2012**, *61*, 1294.
12. Antonioli, D.; Laus, M.; Zuccher, G.; Kapeliouchko, V.; Righetti, M. C.; Boarino, L.; Sparnacci, K. *J. Nanotechnol.* **2012** Article ID 875815.
13. Antonioli, D.; Laus, M.; Sparnacci, K.; Deregibus, S.; Kapeliouchko, V.; Poggio, T.; Zuccheri, G.; Passeri, R. *Macromol. Symp.* **2012**, *311*, 70.
14. Flory, A. L.; Ramanathan, T.; Brinson, L. C. *Macromolecules* **2010**, *43*, 4247.
15. Lu, H.; Nutt, S. *Macromol. Chem. Phys.* **2003**, *204*, 1832.
16. Boucher, V. M.; Cangialosi, D.; Alegria, A.; Colmenero, J. *Macromolecules* **2010**, *43*, 7594.
17. Ash, B. J.; Siegel, R. W.; Schadler, L. S. *J. Polym. Sci. Part B, Polym. Phys.* **2004**, *42*, 4371.
18. Sun, Y.; Zhang, Z.; Moon, K.-S.; Wong, C. P. *J. Polym. Sci. Part B, Polym. Phys.* **2004**, *42*, 3849.
19. Antonioli, D.; Sparnacci, K.; Laus, M.; Boarino L.; Righetti, M. C. *Polym. Compos.* DOI:10.1002/pc22444.
20. Antonioli, D.; Laus, M.; Sparnacci, K.; Deregibus, S.; Kapeliouchko, V.; Palamone, G.; Poggio, T.; Zuccheri, G.; Passeri, R. *Macromol. Symp.* **2010**, *296*, 197.
21. Poggio, T.; Kapeliouchko, V.; Arcella, V.; Marchese, E. *Prog. Org. Coat.* **2003**, *48*, 310.
22. Sarge, S. M.; Hemminger, W.; Gmelin, E.; Hohne, G. W. H.; Cammenga, H. K.; Eysel, W. *J. Therm. Anal.* **1997**, *49*, 1125.
23. Ariawan, A. B.; Ebnesajjad, S.; Hatzikiriakos, S. G. *Polym. Eng. Sci.* **2002**, *42*, 1247.
24. Brown, E. N.; Dattelbaum, D. M. *Polymer* **2005**, *46*, 3056.
25. Chen, B.; Wang, J.; Yan, F. *Tribol. Lett.* **2012**, *45*, 387.
26. ATHAS Data Bank, Pyda M (ed) http://athas.prz.edu.pl/
27. Lau, S. F.; Wesson, J. P.; Wunderlich, B. *Macromolecules* **1984**, *17*, 1102.
28. Varma-Nair, M.; Jin, Y.; Wunderlich, B. *Polymer* **1992**, *33*, 5272.
29. Pompe, G.; Häußler, L.; Pötschke, P.; Voigt, D.; Janke, A.; Geißler, U.; Hupfer, B.; Reinhardt, G.; Lehmann, D. *J. Appl. Polym. Sci.* **2005**, *98*, 1308.
30. Koutsky, J. A.; Walton, A. G.; Baer, E. *J. Appl. Phys.* **1967**, *38*, 1832.
31. Everaert, V.; Groeninckx, G.; Aerts, L. *Polymer* **2000**, *41*, 1409.
32. Balsamo, V.; Gouveia, L. M. *J. Polym. Sci. Part B, Polym. Phys.* **2007**, *45*, 1365.
33. Chen, H. L.; Wu, J. C.; Lin, T. L.; Lin, J. S. *Macromolecules* **2001**, *34*, 6936.

34. Laus, M.; Sparnacci, K.; Antonioli, D.; Deregibus, S.; Kapeliouchko, V.; Palamone, G.; Poggio, T.; Zuccheri, G.; Passeri, R. *J. Polym. Sci. Part B, Polym. Phys.* **2010**, *48*, 548.

35. Alcoutlabi, M.; McKenna, G. B. *J. Phys.: Condens. Matter* **2005**, *17*, R461.

36. Hergeth, W.-D.; Steinau, U.-J.; Bittrich, H.-J.; Simon, G.; Schmutzler, K. *Polymer* **1989**, *30*, 254.

37. Tsagaropoulos, G.; Eisenberg, A. *Macromolecules* **1995**, *28*, 6067.

38. Arrighi, V.; McEwen, I. J.; Quian, H.; Serrano Prieto, M. B. *Polymer* **2003**, *44*, 6259.

39. Sargsyan, A.; Tonoyan, A.; Davtyan, S.; Schick, C. *Eur. Polym. J.* **2007**, *43*, 3113.

40. Barlow, J. W.; Paul, D. R. *J. Polym. Sci. Polym. Lett.* **1985**, *23*, 395.

41. Reinsch, V. E.; Rebenfeld, L. *J. Appl. Polym. Sci.* **1996**, *59*, 1913.

42. Thirtha, V.; Lehman, R.; Nosker, T. *Polymer* **2006**, *47*, 5392.

43. Saleem, A.; Frormann, L.; Iqbal, A. *Polym. Compos.* **2007**, *28*, 785.

44. Aurilia, M.; Sorrentino, L.; Sanguigno, L.; Iannace, S. *Adv. Polym. Tech.* **2010**, *29*, 146.

45. Lewis, T. B.; Nielsen, L. E. *J. App. Polym. Sci.* **1970**, *14*, 1449.

46. Goyanes, S. N.; Konig, P. G.; Marconi, J. D. *J. App. Polym. Sci.* **2003**, *88*, 883.

47. Vassileva, E.; Friedrich, K. *J. App. Polym. Sci.* **2003**, *89*, 3774.

48. Nielsen, L. E.; Wandel, R. W. Mechanical Properties of Polymers and Composites; Marcel Dekker: New York, **1994**.